The Astronomical Journal, 136:51–66, 2008 July doi:10.1088/0004-6256/136/1/51

A LARGE-SCALE OPTICAL–NEAR-INFRARED SURVEY FOR BROWN DWARFS AND VERY LOW MASS STARS IN THE ORION OB1 ASSOCIATION

Juan José Downes[1,2], César Briceño[1], Jesús Hernández[1,3], Nuria Calvet[3], Lee Hartmann[3], and Ernesto Ponsot Balaguer[4]
[1] Centro de Investigaciones de Astronomía, Apartado Postal. 264, Mérida 5101-A, Venezuela; jdownes@cida.ve, briceno@cida.ve
[2] Escuela de Física, Universidad Central de Venezuela, Apartado Postal 47586, Caracas 1041-A, Venezuela
[3] Department of Astronomy, University of Michigan, 825 Dennison Building, 500 Church Street, Ann Arbor, MI 48109, USA; hernandj@umich.edu, ncalvet@umich.edu, and lhartm@umich.edu
[4] Facultad de Ciencias Económicas y Sociales, Universidad de los Andes, Mérida, 5101, Venezuela; ernesto@ula.ve
Received 2007 September 28; accepted 2008 April 8; published 2008 May 27

ABSTRACT

We report the initial results of a large-scale optical–near-infrared (IR) survey to extend the known young population of the entire Orion star-forming region down to the substellar domain. Using deep optical I-band photometry and data from the Two Micron All Sky Survey (2MASS), we selected candidates across ∼14.8 deg^2 in the ∼8 Myr old Ori OB1a subassociation and over ∼6.7 deg^2 in the ∼3 Myr old Ori OB1b subassociation, with completeness down to 0.05 $M_\odot$ and 0.072 $M_\odot$ respectively. We obtained low-resolution optical spectra for a subsample of four candidates in Ori OB1a and 26 in Ori OB1b; as a result we confirmed three new members in Ori OB1a, one of which is substellar, and 19 new members in Ori OB1b, out of which seven are at the substellar limit and five are substellar. We looked into the presence of accretion signatures by measuring the strength of the Hα emission line. Accordingly, we classified the new members as having Classical T-Tauri star-like (CTTS) or Weak Lined T Tauri star-like (WTTS) nature. We found that all the new members confirmed in Ori OB1a are WTTSs, while 39^{+25}_{-22}% of the new members in Ori OB1b exhibit CTTS-like behavior, suggestive of ongoing accretion from a circum(sub)stellar disk. Additionally we found that none of the members confirmed in OB1a shows near-IR color excess while 38^{+26}_{-21}% of OB1b members show $H - K$ color excess. These results are consistent with recent findings for low-mass young stars in Orion OB1. The similarity in CTTS-like properties and near-IR excess across the substellar boundary gives support to the idea of a common formation mechanism for low-mass stars and at least the most massive brown dwarfs. Finally, we comment on the discovery of two new members classified as CTTSs, both exhibiting W(Hα) $\lesssim -140$ Å, suggesting significant ongoing accretion.

Key words: open clusters and associations: individual (Orion OB1) – stars: formation – stars: low-mass, brown dwarfs

Online-only material: color figure

1. INTRODUCTION

One of the main goals of contemporary astrophysics is understanding the processes of star and planet formation. In this context, the formation of the least-massive stars and brown dwarfs (BDs) is a key issue. Because BDs are objects with masses intermediate between those of stars and planets (0.072 $M_\odot \gtrsim M \gtrsim$ 0.010 $M_\odot$; Baraffe et al. 1998; Oppenheimer et al. 2000), understanding how they form can provide important links between the origin of stars and planetary bodies.

Current observational efforts seek to establish to what extent there is a continuity of the star-formation process across the substellar limit ($M \sim 0.072 M_\odot$; Baraffe et al. 1998), and whether the properties of the resulting (sub)stellar populations depend on aspects like the surrounding environment. Observational evidence shows that for some very young populations the kinematic and spatial distributions of very low mass stars (VLMSs) and BDs are similar, that there is continuity of the initial mass function between VLMSs and BDs with masses down to 0.02$M_\odot$ (Luhman et al. 2007, 443–457), and that BDs accrete from circumsubstellar disks, much like low-mass stars do (e.g., Jayawardhana et al. 2002; Muzerolle et al. 2005). These results suggest that the low-mass star-formation process extends across and below the substellar limit. However, these findings are based on observations of regions with ages between 1 and 2 Myr (Taurus, IC348, Trapezium, and Chameleon I), much younger than the ∼10 Myr time span in which giant planets are expected to form (Calvet et al. 2005). Also, these studies do not offer clear evidence on the dependence (if any) of the formation processes with the environment, because they compare different regions which do not share a common origin.

An important and required next step is the detection, minimizing spatial biases, of stellar and substellar pre-main-sequence (PMS) populations in star-forming regions that show a variety of environmental conditions, span an age range from ∼1 to 10 Myr, and ideally share the same "genetic" pool. Such samples can offer new insights into the formation and evolution of BDs: (a) the time dependence of indicators of disks and of disk accretion, over a span of 10 Myr, will offer the best view yet of how disks evolve, under a diversity of environments and at both sides of the substellar limit; (b) the space distribution and kinematics of these populations will provide important constraints to the formation models, e.g., the dynamical ejection scenario (Reipurth & Clarke 2001), which suggests that BDs are stellar embryos ejected from their birthplaces as a consequence of dynamical interactions during the early stages of their formation, resulting in them being deprived from gaining mass from the surrounding gas.

The Orion star-forming region meets all these requirements. It is a relatively nearby OB association (∼400 pc; Briceño

et al. 2005), representative of the birthplace for the majority of stars in our Galaxy (Briceño et al. 2007a), containing regions with ages $\sim 1 - 10$ Myr and differing ambient conditions (Genzel & Stutzki 1989; Briceño et al. 2005). There is also a molecular cloud complex (Maddalena et al. 1986), in which the youngest star populations are embedded, which shares the same kinematics as the older stars (Briceño et al. 2007b, 345–360), suggesting that the stellar populations at various ages share a common origin. Throughout the whole region there is now a significant number of confirmed PMS stellar members (Briceño et al. 2005, 2007b, 345–360); however, substellar objects have only been confirmed so far in the younger, densest regions with small spatial extent, such as the σ Ori cluster (e.g., Béjar et al. 1999, 2001; Barrado y Navascués et al. 2003a; Caballero et al. 2004; Sherry et al. 2004; Kenyon et al. 2005; González-García et al. 2006) or the Orion Nebula Cluster (Hillenbrand & Carpenter 2000; Preibisch et al. 2005; Slesnick et al. 2005). In order to look for the faintest, lowest-mass members widely distributed across the Orion OB1 association, down to and beyond the substellar limit, we are conducting a large-scale optical–near-infrared (IR) search for BDs that spans $\sim$180 deg^2 over the entire region. Our strategy is to combine deep, co-added, R-band, and I-band data from our optical photometry obtained with the QUEST I CCD Mosaic Camera in Venezuela (Briceño et al. 2005), with near-IR measurements from the Two Micron All Sky Survey (2MASS) to select objects, which we call candidates, whose photometric magnitudes and colors are consistent with those of BDs and VLMSs. We then obtain follow-up spectra to confirm membership and establish their stellar or substellar status. Finally, we characterize objects in terms of spectroscopic signatures such as strong Hα emission, which we use as a proxy for ongoing disk accretion.

In this work we present initial results in this effort to extend the known young population of the entire Orion star-forming region throughout the substellar limit. We selected optical–near-IR candidates within an area of $\sim$21 deg^2, encompassing part of the Orion OB1a and most of the Orion OB1b subassociations. We conducted spectroscopic follow-up of candidates in an area of 0.8 deg^2 in OB1a, and 2.5 deg^2 in OB1b. The optical photometric observations are described in Section 2. Candidate selection was done by defining regions in optical–near-IR color–magnitude and color–color diagrams, as explained in Section 3. Section 4 shows the results of the spectroscopic observations and spectral classification of a first sample of candidates, covering $\sim$3.3 deg^2. The criteria followed to establish membership and the stellar or substellar nature of the candidates are presented in Section 5. In Section 6 we study the spectral types and Hα emission in order to classify the new BDs and VLMSs according to their Weak Lined T Tauri star-like (WTTS) or Classical T Tauri star-like signatures (CTTS), and compare the fraction of both types of objects with previous results obtained in the stellar low-mass regime ($0.25 \lesssim M/M_\odot \lesssim 0.9$) of the same region (Briceño et al. 2005, 2007b, 345–360). In Section 7 we discuss the IR emission properties of the new members, and compare with similar mass objects confirmed as members in other subregions of Orion. In Section 8 we estimate the extinctions, temperatures, luminosities, and masses and plot the newly confirmed members in $H-R$ diagrams. Finally in Section 9 we summarize the results and conclusions.

2. PHOTOMETRY

2.1. Co-adding of Optical Images

Since 1998 a multi-band (Johnson-Cousins BVRI) and multi-epoch large-scale survey ($\sim$180 deg^2) of the Orion star-forming region ($5h < \alpha < 6h$, $-6^\circ < \delta < 6^\circ$) has been performed with the Jürgen Stock 1.0/1.5 Schmidt-type telescope and the QUEST-I camera, at the Venezuela National Astronomical Observatory. The camera was developed by the QUEST collaboration (Baltay et al. 2002) and consists of 16 2048 × 2048 pixel CCDs in a 4 × 4 array which, taking into account the gaps between CCDs, provides a field of view of 5.4 deg^2 with a scale of $\sim$1.02 arcsec pixel^{-1}. The system is optimized for observations performed in drift-scan mode at declinations near to the celestial equator. In this mode of operation, the telescope is fixed while the sidereal motion is compensated for by adjusting the angle of each row of CCDs, which ride on a common supporting Invar rod, and by fine-tuning the readout frequency for each chip. Each CCD row is oriented in the north–south direction and is provided with a filter, resulting in a quasi-simultaneous observation in four different filters with an integration time per filter of 140 s at $\delta = 0^\circ$. Thus, the system produces scans at a rate of $\sim$34.5 deg^2 h^{-1} per filter.

Table 1
Observation Log of the Individual Scans Used to Produce the Co-added Scan

Date	Scan	$\alpha_i(J2000)$	$\alpha_f(J2000)$	Filters	Mean seeing ($''$)
1998 Dec 13	504	04:10:00	05:51:00	RBIV	2.81
1998 Dec 13	505	04:10:00	05:51:00	RBIV	2.95
1998 Dec 29	501	04:10:00	05:51:00	RBIV	2.91
1998 Jan 9	527	03:55:00	05:53:00	RBIV	2.93
1999 Jan 9	528	03:55:00	05:53:00	RBIV	2.92
1999 Jan 10	529	03:55:00	05:53:00	RBIV	2.85
1999 Jan 9	528	03:55:00	05:53:00	RBIV	2.92
1999 Jan 10	529	03:55:00	05:53:00	RBIV	2.85
1999 Jan 10	530	03:55:00	05:53:00	RBIV	2.95
1999 Jan 22	501	03:55:00	05:53:00	RBIV	3.06

Our main interest is the analysis of existing I-band observations, for which the system attains a limiting magnitude $I_{\rm lim} \sim 19.5$, with a completeness limit of $I_{\rm com} \sim 18.5$. In order to evaluate the faintest magnitude at which we could expect the substellar limit to correspond for each of the regions spanned by our optical data, allowing for uncertainties in ages, distance, and reddening, we made the following estimates. Using the models of Baraffe et al. (1998), the substellar limit for OB1a on the 12.6 Myr isochrone is placed at $I \sim 18.1$ (for a distance modulus $(m - M)_{\rm OB1a} = 7.59$ and extinction $A_V = 0.6$; Briceño et al. 2005, 2007b, 345–360), and the substellar limit for Ori OB1b on the 6.3 Myr isochrone is placed at $I \sim 18.1$ too (distance modulus $(m - M)_{\rm OB1b} = 8.21$ and maximum extinction $A_V = 2$; Briceño et al. 2005, 2007b, 345–360). We consider these isochrones as rough upper limits for the age of each subregion based on the age ranges reported by Briceño et al. (2005) for OB1a and OB1b. Because the substellar limit in each region is near the completeness limit of our individual I-band observations, we use a coadding technique in order to increase the signal-to-noise ratio (S/N) and therefore the limiting and completeness magnitudes of our optical data.

For the co-add we selected eight individual (single) scans centered at $\delta = -1^\circ$, that were obtained in the R and I bands between 1998 December and 1999 January. The corresponding observation log is shown in Table 1.[5] The sum was performed using the packages `Offline` (Baltay et al. 2002) and `DQ` developed by the QUEST collaboration. `Offline` automatically

[5] This publication makes use of the Sistema de Colección de Datos Observacionales del Telescopio Schmidt version 2000 (SCDObs2000; Ponsot et al. 2007).

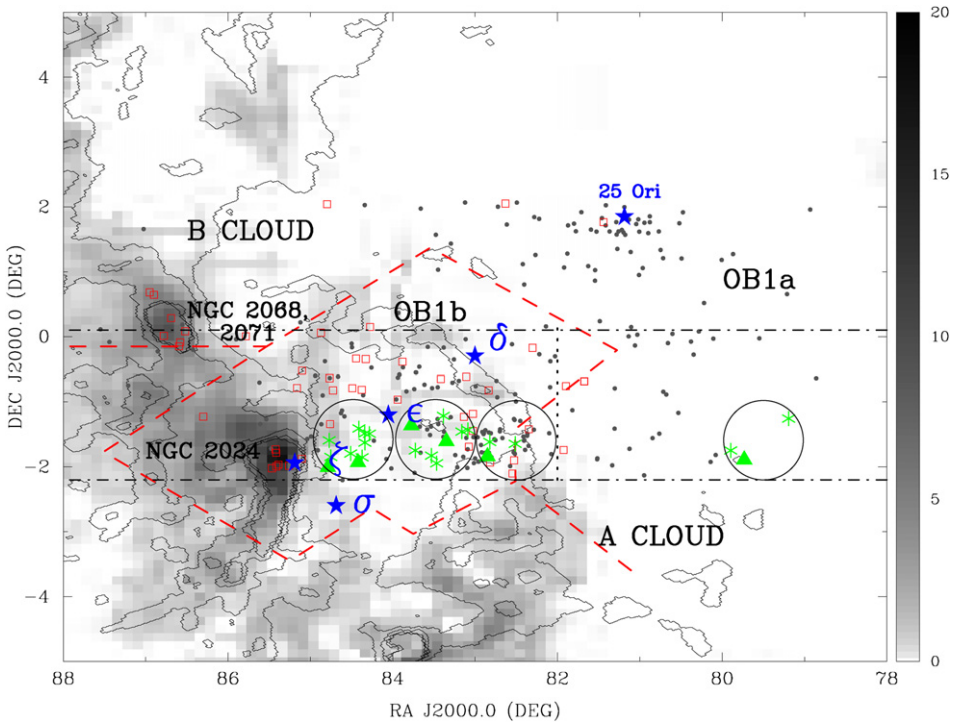

Figure 1. Spatial location of the newly discovered VLMSs and BDs. The triangles and stars indicate BDs and VLMSs respectively, spectroscopically confirmed as members within the Hectospec fields (solid line circles). Members classified by Briceño et al. (2005, 2007b, 345–360) as CTTSs are indicated with small empty squares and WTTSs with filled dots. The horizontal dot-dashed lines indicate the north and south limits of our scans centered at $\delta_{J2000.0} = -1.0°$. The dashed line region marks the boundary of the OB1b and OB1a regions as defined by Warren & Hesser (1977). The dotted vertical line indicates the adopted spatial limit between OB1a and OB1b subregions into the strip of our photometric sample as we explained in Section 2.1. The gray scale map shows the integrated ^{13}CO emissivity from Bally et al. (1987). The isocontours correspond to the dust extinction map of Schlegel et al. (1998), in $E(B-V)$ steps of 0.1–1.5 mag.

(A color version of this figure is available in the online journal)

processes an individual scan considering each CCD of the array as an independent device, reducing the images by bias, dark current, and flat field, using calibration images obtained in drift-scan mode during the observation runs (see Baltay et al. 2002 for further details on the reduction process). After these corrections, `Offline` performs the detection of point sources, aperture photometry, and finally computes the astrometric matrix for each CCD image, based on the USNOA-2.0 catalog (Monet et al. 1998). `DQ` processes the raw scans, regarding each CCD from different scans as independent devices; then does the bias subtraction, dark current, and flat-field corrections, following the same procedure as employed by `Offline`. Using the astrometric matrices produced by `Offline`, the `DQ` software computes the offsets, rotations, and scale differences between images of the same area of the sky obtained from different scans. With these corrections `DQ` produces, for each scan, a new output "scan" composed by a set of processed images that can be added pixel by pixel to produce the final co-added scan. The final gain in depth is ∼1 mag and the resulting co-added scan encompasses the region $75° < \alpha < 85°$, $-2.2° < \delta < 0.1°$ for the R and I filters.

Our first step in defining the photometric candidate sample is the selection in I versus $I - J$ diagrams of objects located above the isochrone that defines the upper age limit for each subassociation, because it is in these regions of the color–magnitude diagrams that the PMS populations are expected to fall. Because of the differences in age and distance we need to apply this procedure independently for each subassociation, which requires the definition of a spatial limit between the two. Using the integrated ^{13}CO emissivity observed in the region by Bally et al. (1987), and the isocontours corresponding to the dust extinction map of Schlegel et al. (1998), as indicators of the position of the molecular clouds associated with OB1b, we considered $\alpha \sim 82$ deg as the rough limit between OB1a and OB1b within the 2.3 deg wide strip spanning the photometric sample analyzed in this work. This spatial limit between the two subassociations is consistent with that discussed by Briceño et al. (2005), who consider the molecular ringlike structure roughly centered on the Orion Belt star ϵ Ori, as a good tracer of the extent of the OB1b subassociation; within this gas ring are found the majority of low-mass PMS stars classified by them as members of OB1b. Figure 1 shows part of the entire area of our Orion optical survey, as well as the strip centered at $\delta_{J2000.0} = -1°$ considered here, the dust extinction map and ^{13}CO emissivity used to define the limit between both regions and the fields of the spectroscopic follow-up analyzed in this work.

2.2. Optical Photometry and 2MASS Data

The detection of point sources in the coadded scan was performed with the `daofind` task in IRAF[6], extracting objects with R- and I-band fluxes above $3\sigma_{\rm sky}$. The small amount of crowding in our images (∼1.4 sources arcmin^{-2}) justifies the use of aperture photometry. We used the `phot` task in IRAF,

[6] IRAF is distributed by the National Optical Astronomy Observatory, which is operated by the Association of Universities for Research in Astronomy, Inc., under cooperative agreement with the National Science Foundation.

adopting an aperture radius (computed from growth curves) of 4″, which is ∼1.4 times the typical FWHM in both bands. Because our pixel scale is 1″ and the typical FWHM of the images is 2.5″ − 3″, each stellar profile is well sampled.

The astrometric solutions were computed using the WCStools package (Mink 1999). and astrometric standards of the Guide Star Catalog GSCII,[7] yielding a median offset between R-band and I-band catalogs of 0.89″ with a standard deviation of 0.78″.

The photometric calibration to the Cousins system was performed by defining a set of 416 *secondary photometric standards*, located in four fields within our $\delta_{J2000.0} = -1^{\circ}$ Orion strip. We made sure that each of the four strips at constant declination that compose a single driftscan observation, as produced by each of the four rows of detectors in the QUEST-I camera, would enclose roughly 100 of these secondary standard stars. The stars were chosen as objects known not to be variable from our multi-epoch survey data; only those flagged as non-variable at the $\leqslant$0.05 mag level were used. The secondary standards span a range of brightness but are not saturated in any single observation, and they are not too faint, so that each star would yield an S/N $\gtrsim$ 50. The secondary standards were in turn calibrated using 12 primary photometric standard stars located in the SA92 and PG0231 Landolt fields (Landolt 1992), observed at various airmasses under photometric conditions, with the 4-SHOOTER CCD camera on the 1.2 m telescope at the Smithsonian Astrophysical Observatory. The seeing was ∼2″ throughout the observations. The 4-SHOOTER camera contains four 2048 × 2048 Loral CCDs separated by 45″ and arranged in a 2 × 2 grid. After binning 2 × 2 during readout, the plate scale was 0.67″ pixel^{-1}. In order to achieve more uniform and consistent measurements, we placed all the standard stars on the same CCD detector (chip 3). Bias and flat-field corrections were applied to the raw images using the standard tasks in the IRAF `ccdproc` package. We then performed aperture photometry with the `apphot` package, and derived zero points, extinction coefficients, and color terms using the `photcal` package. The photometric errors of the secondary photometric standard stars are $\sigma < 0.05$ in the R- and I-bands.

The calibration of sources from the coadded images was performed independently for each CCD using standard IRAF tasks, yielding a root mean square (rms) = 0.037 mag and 0.042 mag in the R- and I-bands, respectively. Sources without detections in the R-band were calibrated independently in the I-band using zero points only. Therefore, we obtained two sets of data calibrated in different ways: one including an $R-I$ color term and the other without it. In the transformation equation used to convert instrumental magnitudes to the secondary standard star system, the $R - I$ color coefficient has a rather small mean value of −0.046 for the I-band. The observed $R - I$ color of the candidates is in the interval $1.24 < R - I < 2.4$; therefore, the difference between I magnitudes computed using a color term and those computed without it is 0.05 mag for the bluest and brighter candidates (expected to have an $\sim M3$ spectral type) and 0.11 mag for the reddest and fainter candidates (expected to have an $\sim M7$ spectral type). The final optical data catalog includes ∼223,000 objects with typical instrumental errors of $0.04 < \sigma_I \leqslant 0.2$ at $19 \geqslant I \geqslant I_{\rm lim}$ and $0.05 < \sigma_R \leqslant 0.2$ at $20 \geqslant R \geqslant R_{\rm lim}$. Therefore, the calibration using secondary standard stars offers adequate photometric accuracy for the VLMSs and substellar candidate selection and the subsequent analysis presented at this study. The 3σ limiting magnitudes obtained are $R_{\rm lim} = 21.5$ and $I_{\rm lim} = 20.7$, with completeness limits of $R_{\rm com} = 20.3$ and $I_{\rm com} = 19.0$. We define here completeness as the value at which the magnitude distribution departs from a linear behavior. Saturation occurs at $R_{\rm sat} \sim I_{\rm sat} \sim 13.5$.

A total number of ∼127,000 sources were observed in our survey region by the 2MASS project, with limiting magnitudes of $J_{\rm lim} = 18.9$, $H_{\rm lim} = 18$, $K_{\rm lim} = 17.4$ and completeness limits of $J_{\rm com} = 16.6$, $H_{\rm com} = 16$, $K_{\rm com} = 15.4$ computed following the same procedure used for our optical data. Typical uncertainties in the 2MASS data are $0.1 < \sigma_{J,H,K} < 0.5$ between completeness and limiting magnitudes for the three bands. A total number of ∼106,000 objects from the optical catalog were identified in the 2MASS data, resulting in a median offset between both catalogs of 1.41″ with a standard deviation of 0.89″.

3. CANDIDATE SELECTION

The candidate selection was performed using optical–IR color–magnitude and color–color diagrams. This method has proved successful in identifying VLMS and BD candidates in young clusters and various star-forming regions (Briceño et al. 2002; Luhman et al. 2003a).

We compared the optical and IR magnitudes and colors with isochrones and evolutionary tracks from Baraffe et al. (1998) models, in diagrams that included I-, J-, H-, and K-band data. As mentioned in Section 2.1, we assumed a distance modulus of $(m - M)_{\rm OB1a} = 7.59$ for OB1a, and $(m - M)_{\rm OB1b} = 8.21$ for OB1b (Briceño et al. 2005). The first step was the selection in the I versus $I - J$ diagram of objects placed above isochrones assumed to be a reasonable upper age limit for each subassociation, 12.6 Myr for OB1a and 6.3 Myr for OB1b (Section 2.1). In addition, because we are interested here in the lowest-mass PMS stars and BDs, we required that candidates be located below the 0.3 $M_{\odot}$ evolutionary track of the Baraffe et al. (1998) models.[8] These diagrams are shown in Figure 2. The objects selected from the I versus $I - J$ diagrams were then plotted on the H versus $I - K$ plane. There we checked their positions with respect to the same isochrones and evolutionary tracks as we used in the I versus $I - J$ diagrams, in order to verify the consistency of the first selection step. Finally, in order to reduce the contamination from reddened early-type (and therefore more massive) stars, we selected only objects located above the reddening line corresponding to a spectral-type M5 in the $I - K$ versus $J - H$ diagrams shown in Figure 3. On average, only objects later than M5 ($M < 0.1\ M_{\odot}$), at different reddening values, are expected in this region of the diagram as we show in Figure 3.

The reddening lines and vectors were computed according to the Cardelli et al. (1989) extinction law with $R_V = 3.1$ (representative of OB associations), Baraffe et al. (1998) models, and temperature–spectral-type relationships from Luhman et al. (2003b). The resulting catalog includes 64 VLMS candidates in OB1a and 118 in OB1b, and 58 BD candidates in OB1a and 77 in OB1b. Based on the completeness limits in the I- and J-bands, and Baraffe et al. (1998) models, we estimate the photometric sample to be complete down to members with masses 0.05 $M_{\odot}$ with $A_V \leqslant 0.6$ for OB1a, and masses 0.072 $M_{\odot}$ for

[7] The Guide Star Catalog was produced at the Space Telescope Science Institute under U.S. Government grant. These data are based on photographic data obtained using the Oschin Schmidt Telescope on Palomar Mountain and the UK Schmidt Telescope.

[8] The census and study of the Orion OB1 PMS stars with masses above 0.3 $M_{\odot}$ is the subject of works such as Briceño et al. (2001, 2005).

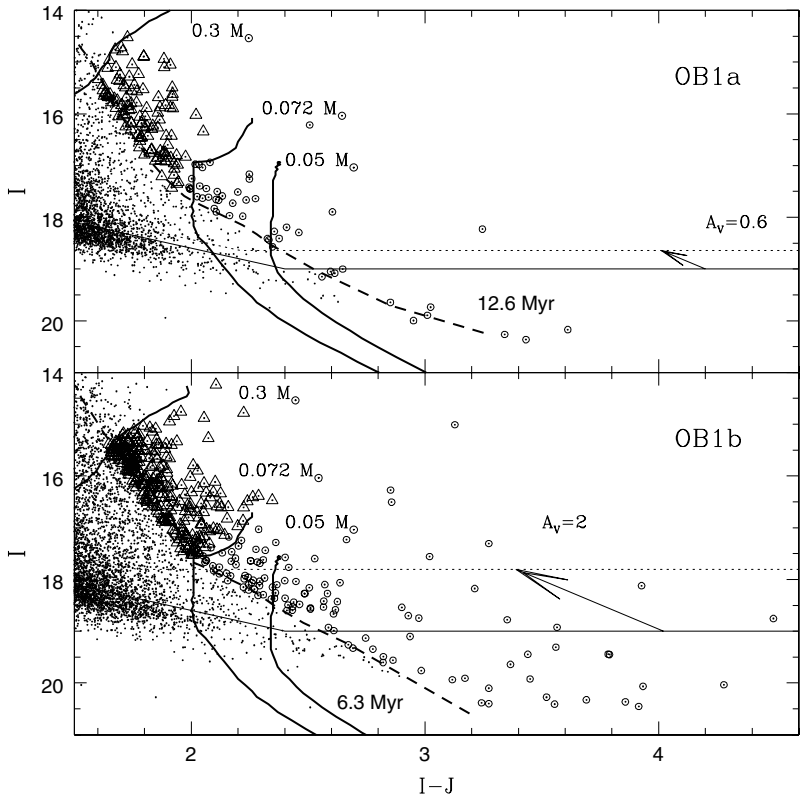

Figure 2. First selection of candidates. The dots represent field sources located under the isochrone that defines the upper age limit of each region, based on results from Briceño et al. (2005) (12.6 Myr for OB1a and 6.3 Myr for OB1b; dashed lines), or PMS candidates located above the 0.3 $M_\odot$ evolutionary track that were rejected as candidates. Sources above the isochrones, between the 0.3 $M_\odot$ and 0.072 $M_\odot$ evolutionary tracks (open triangles), and below the substellar limit (0.072 $M_\odot$ evolutionary track; open circles), were selected as initial candidates. The thin solid lines represent the completeness of the photometric sample, and the dotted lines show the completeness assuming $A_V = 0.6$ for OB1a, and $A_V = 2$ for OB1b. These extinctions correspond to the representative upper values measured in our spectroscopic sample for each region, resulting in a mass completeness of ∼0.05 $M_\odot$ for OB1a and ∼0.072 $M_\odot$ for OB1b. We used models from Baraffe et al. (1998) and a distance modulus of 7.59 for OB1a, and 8.21 for Ob1b (Briceño et al. 2005). The reddening vectors were computed using the Cardelli et al. (1989) extinction law with $R_V = 3.1$, and temperature–spectral-type relationship from Luhman et al. (2003a).

OB1b with $A_V \leqslant 2$ as we show in Figure 2. Both reddening values are representative of the typical upper limits measured on our spectroscopic sample (see below) and in low-mass stars confirmed in both subregions by Briceño et al. (2005, 2007a).

4. OPTICAL SPECTROSCOPY

4.1. Spectroscopic Observations

Though the photometric candidate selection technique is particularly sensitive to young VLMS and BD, a fraction of ∼25–30% of the sample is expected to be composed of background and foreground objects, contaminating the candidate lists. Actually, the field dwarfs 2MASS 05395200-0059019 (L5V; Fan et al. 2000) and the 2MASS 05012406-0010452 (L4V; Gelino et al. 2004) were detected in our photometric survey with $R = 20.27 \pm 0.16$, $I = 17.32 \pm 0.01$ ($R - I = 2.95$), and $R = 20.14 \pm 0.08$, $I = 18.23 \pm 0.02$ ($R - I = 1.91$) respectively and are included in our candidate list. Also, background late-type giants may be present. Therefore, spectroscopic confirmation of membership to the association is necessary.

We obtained low-resolution spectra of a first sample composed of 30 objects: four candidates are located in OB1a and 26 in OB1b. We used the Hectospec multi-fiber spectrograph on the 6.5 MMT telescope (Fabricant et al. 1998). In its $f/5$ configuration the telescope offers a ∼0.8 deg^2 field of view, in which 300 fibers of the spectrograph can be placed. We used the 270 groove mm^{-1} grating that provides a spectral resolution of 6.2 Å with a spectral coverage from 3700 to 9150 Å. Each fiber subtends 1.5″ on the sky and requires accurate coordinates for positioning. We used 2MASS coordinates for all our candidates.

The observations were performed as part of the spectroscopic follow-up of the CIDA Variability Survey of Orion (Briceño et al. 2005) in which the main goal is the identification of low-mass stars in the range $0.2 < M/M_\odot < 0.9$. Because of this, the spatial coverage in each OB1a and OB1b was dictated by the number of fields observed with Hectospec in each region for the shallow survey, out of which only fields containing VLMS and BD candidates from our deep co-add are considered here. The four candidates located in OB1a all fall within one Hectospec field, spanning ∼0.8 deg^2. The 26 objects in OB1b are distributed over a larger area of ∼2.5 deg^2 (three Hectospec fields). For all fields the total integration time was 3 × 900 s. Because in Hectospec all objects placed in the same field have the same integration time, many of our faint VLMSs and BDs candidates had low S/N. However, this did not affect in a significant way the spectral classification as we explain in the following section.

All the spectra were processed, extracted, and wavelength calibrated by S. Tokarz at the CfA Telescope Data Center, using

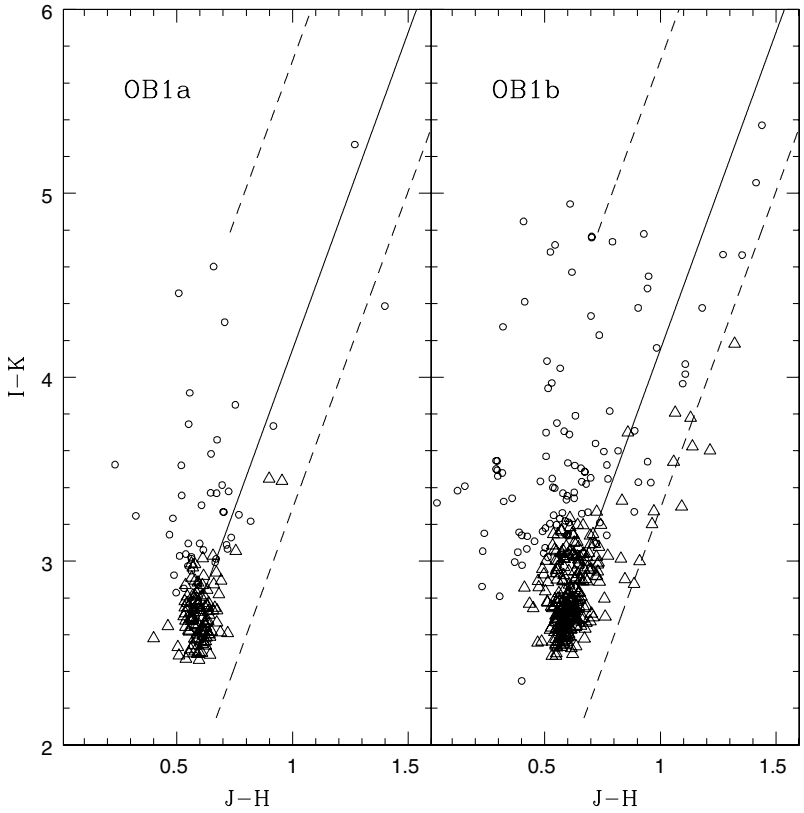

Figure 3. Final step in the selection of candidates. The symbols are the same as in Figure 2. The solid lines represent the reddening line for M5 objects and the dashed lines the reddening lines for M1 (lower) and M9 (upper) objects, computed using the Cardelli et al. (1989) extinction law with $R_V = 3.1$, Baraffe et al. (1998) models, and temperature–spectral-type relationships from Luhman et al. (2003a). On average, sources falling above the M5 reddening line are later than M5 at different A_V values and were selected as final candidates.

Table 2
Hectospec Observation Log

Date	Subregion	Field ID	$\alpha(J2000)$	$\delta(J2000)$	Integration (seg)
2005 Apr 9	OB1a	decm160_04	05:17:59.67	−01:35:19.4	2700
2004 Nov 3	OB1b	decm160_07	05:30:00.47	−01:35:33.7	2700
2005 Mar 4	OB1b	decm160_08	05:33:55.64	−01:34:29.8	2700
2004 Nov 19	OB1b	decm160_09	05:37:55.32	−01:34:33.0	2700

customized IRAF routines and scripts developed by the Hectospec team. A typical number of 37 fibers per field were used to obtain sky spectra; these were combined and the resulting spectra were subtracted from the target spectra. The fields in the OB1b subassociation were selected far enough from the the molecular clouds to avoid problems due to the high sky background caused by nebulosity; however, some objects placed in the easternmost OB1b field do show some contamination by cloud emission lines (although these lines did not affect the spectral classification). The spectra were wavelength calibrated using arc lamp data. The appropriate correction for the sensitivity function of the detector was applied, and the effects of the atmospheric extinction were computed, using standard IRAF routines based on observations of the spectrophotometric standard star BD+284211. Light sources inside the fiber positioner of Hectospec contaminate ∼1/3 of the fibers at the red edge, starting at ∼8500 Å (N. Caldwell 2007, private communication); therefore, during the analysis we ignored data at wavelengths beyond this value. The observations log is shown in Table 2.

4.2. Spectral Classification

We performed the spectral classification based on the comparison with of temperature-sensitive spectral indices. We extended the semi-automated procedures of Hernández et al. (2004) and Sicilia-Aguilar et al. (2005) for their application to VLMSs and BDs, by adding indices measured for the 16 spectral features listed in Table 3, and a library of standard spectra of field dwarfs from Kirkpatrick et al. (1999). Our set of spectral indices spans a wavelength range 4775–7940 Å, including spectral features such as TiO absorption bands that increase in strength from K5 to M7 spectral types, and VO absorption bands that start dominating spectra from M7 to early L types.

Spectral types for noisy spectra were checked directly with the standard star spectral sequence using the visual extinction as a free parameter to get a more accurate result. The classification[9] is shown in Table 4, and Figure 4 shows the spectra, with adopted spectral types of the new members shown in labels.

[9] This procedure has been done using the code SPTCLASS, available at http://www.astro.lsa.umich.edu/∼hernandj/SPTclass/sptclass.html.

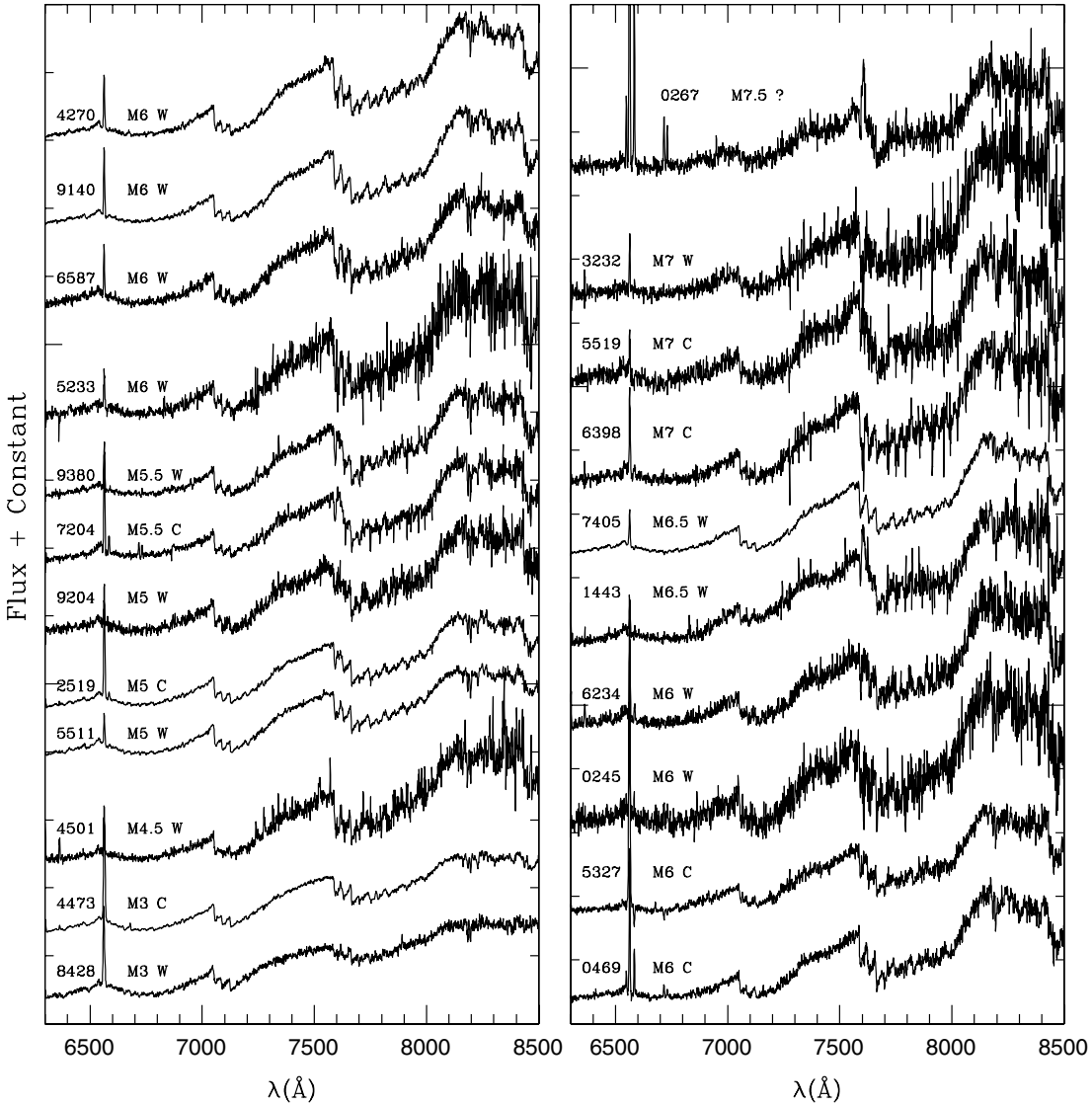

Figure 4. New members confirmed in this work. Each spectrum shows the last four characters of its 2MASS ID, and the spectral type followed by its classification as CTTSs or WTTSs. All spectra were normalized at 7500 Å and are shown at their original resolution of 6 Å. Member 0267 does not have a clear classification as CTTS or WTTS, as is explained in Section 6.1.

Table 3
Spectral Features from Kirkpatrick et al. (1999) Used for the Semi-Automated Spectral Classification

Feature ID	λ_c (Å)	$\Delta\lambda$ (Å)
TiO-1	4775	30
TiO-2	4975	50
TiO-3	5225	75
TiO-4	5475	75
TiO-5	5600	50
TiO-6	5950	75
TiO-7	6255	50
TiO-8	6800	50
TiO-9	7100	50
TiO-10	7150	50
VO-1	7460	100
VO-2	7840	100
VO-3	7940	100

5. ASSOCIATION MEMBERSHIP AND SUBSTELLAR NATURE

5.1. Membership Diagnostics

Candidates classified as late-M-type objects can be divided into three different groups: first, the VLMSs and BDs that belong to the Orion OB1 association; second, background stars composed by late-type giant stars; and third, foreground, old M-dwarf field stars. We have used several criteria to assign Orion OB1 membership to each candidate. These include the location above the zero-age main sequence (ZAMS) in color–magnitude diagrams, A_V values close to the characteristic absorption toward each region, and spectroscopic indicators that characterize young, low-mass objects.

First, we consider the Hα λ6563 line in emission, with equivalent width increasing toward later spectral types (Barrado y

Table 4
Catalog of Very Low Mass Stars and Brown Dwarfs Confirmed as New Members of Orion OB1

2MASS-ID	$R_C \pm \sigma R_C$	$I_C \pm \sigma I_C$	J	H	K	$ST\sigma ST$	adST	W[Hα]	Lines	WTTS/CTTS	Av	Log($L/L_\odot$)	$T_{\rm eff}$	$M(M_\odot)$
05164635-0115233	19.225 ± 0.047	17.121 ± 0.010	14.946	14.415	14.127	M6.0 ± 0.5	M6	−26.8	...	W	0.6	−1.81	2990	0.07
05185578-0153232	20.204 ± 0.100	17.767 ± 0.015	15.364	14.640	14.260	M7.0 ± 1.0	M7	−18.5	...	W	0.5	−1.80	2880	0.06
05193522-0144501	18.706 ± 0.023	16.882 ± 0.007	14.864	14.330	14.020	M4.7 ± 0.5	M4.5	−13.3	...	W	0.9	−1.79	3197	0.15
05300324-0138428	...	16.272 ± 0.013	13.419	12.515	11.895	M2.7 ± 0.5	M3	−20.0	...	W	3.9	−0.64	3415	0.40
05311727-0136587	19.049 ± 0.037	16.989 ± 0.008	14.944	14.432	14.078	M6.0 ± 0.5	M6	−16.8	...	W	0.1	−1.63	2990	0.08
05312373-0150245	19.967 ± 0.066	17.839 ± 0.016	15.643	15.104	14.485	M6.2 ± 0.5	M6	−24.4	...	W	0.6	−1.85	2990	0.07
05322069-0125511	18.376 ± 0.015	16.569 ± 0.005	14.656	14.205	13.709	M4.8 ± 0.5	M5	−8.8	...	W	0.2	−1.56	3125	0.13
05323839-0127204	...	18.059 ± 0.018	15.800	15.298	14.986	M5.5 ± 0.5	M5.5	−26.0	...	C	1.0	−1.91	3057	0.09
05332365-0136234	20.081 ± 0.071	17.819 ± 0.014	15.379	14.856	14.458	M6.0 ± 1.0	M6	−22.3	...	W	1.3	−1.67	2990	0.08
05333251-0112519	18.158 ± 0.024	16.240 ± 0.009	14.013	13.347	12.921	M5.0 ± 1.0	M5	−31.1	...	C	1.2	−1.19	3125	0.17
05335219-0156398	...	18.102 ± 0.024	15.736	14.967	14.579	M7.0 ± 1.5	M7	−207.4	...	C	0.3	−1.73	2880	0.06
05340726-0149380	20.148 ± 0.100	17.876 ± 0.017	15.641	15.271	14.766	M5.5 ± 1.0	M5.5	−10.4	...	W	1.0	−1.83	3057	0.09
05345443-0144473	17.020 ± 0.005	15.773 ± 0.004	13.381	12.511	11.901	M3.0 ± 0.5	M3	−32.8	He I	C	2.5	−0.78	3415	0.40
05350579-0121443	...	18.928 ± 0.040	16.341	15.835	15.229	M6.5 ± 1.0	M6.5	−18.1	...	W	1.4	−2.00	2935	0.07
05370790-0129204	20.344 ± 0.090	18.173 ± 0.017	15.869	15.564	15.216	M4.8 ± 0.5	M5	−4.7	...	W	1.4	−1.91	3125	0.13
05372198-0129140	18.676 ± 0.020	16.484 ± 0.005	14.209	13.703	13.333	M6.1 ± 0.5	M6	−26.8	...	W	0.8	−1.26	2990	0.10
05373853-0124270	18.617 ± 0.026	16.701 ± 0.007	14.592	14.037	13.625	M6.2 ± 0.5	M6	−32.4	...	W	0.3	−1.47	2990	0.09
05374145-0155519	...	18.295 ± 0.031	15.987	15.484	15.115	M7.0 ± 0.5	M7	−47.0	He I	C	0.2	−1.83	2880	0.06
05380232-0147405	18.406 ± 0.020	16.249 ± 0.004	14.088	13.487	13.103	M6.5 ± 0.8	M6.5	−16.5	...	W	0.1	−1.24	2935	0.08
05390054-0150469	19.613 ± 0.065	17.732 ± 0.018	15.476	15.020	14.539	M6.2 ± 1.0	M6	−67.1	...	C	0.7	−1.78	2990	0.07
05390532-0135327	19.604 ± 0.041	17.619 ± 0.011	15.356	14.784	14.454	M5.8 ± 0.5	M6	−140.3	He I	C	0.8	−1.72	2990	0.07
05390910-0200267	...	19.102 ± 0.086	16.166	15.559	15.413	M7.7 ± 1.0	M7.5	−93.5	...	?	1.6	−1.90	2795	0.04

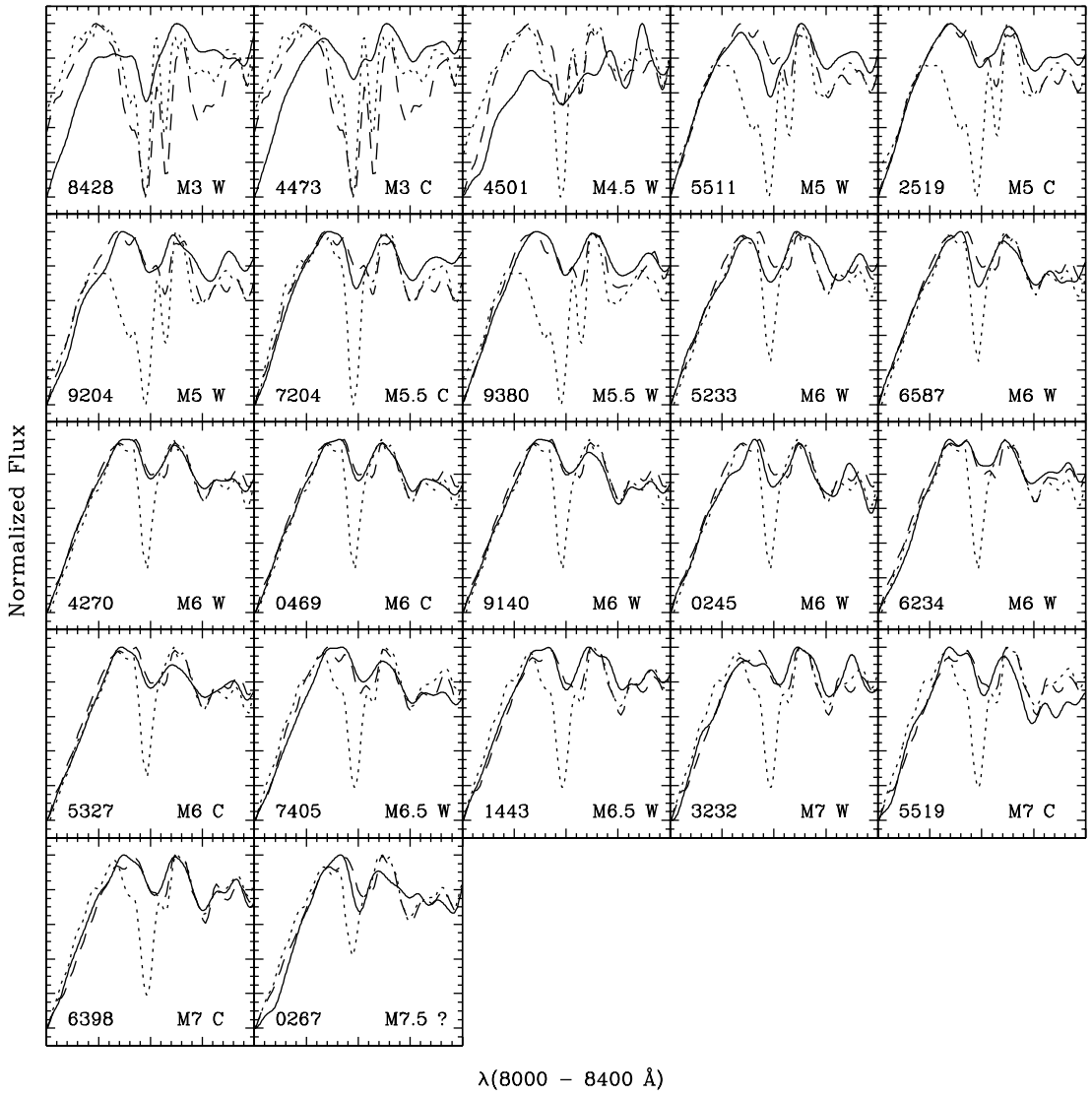

Figure 5. The Na I λ8195 absorption lines in the newly confirmed members (solid line), for field dwarfs (dotted line; Kirkpatrick et al. 1999), and for young VLMSs and BDs from Chamaeleon I region (∼2 Myr; dashed line; Luhman 2004). New members and comparison templates have the same spectral types. All spectra were smoothed to a resolution of 16 Å and normalized in the interval 8000–8400 Å.

Navascués et al. 2003b; White & Basri 2003). Strong Hα emission is a common feature of chromospherically active young objects, and of young objects accreting from a circumstellar disk (for the largest equivalent widths; e.g. Muzerolle et al. 2005). By adopting this criterion we eliminated contamination from background giant stars. Still, Hα emission can occur in dMe stars. In order to distinguish PMS objects from these late-type field stars, and considering that PMS objects are still contracting, we chose as an additional youth indicator the strength of the Na I λ8195 absorption feature. This doublet is sensitive to surface gravity and varies significantly between dwarf field stars and PMS objects; equivalent widths in young M dwarfs fall between those of field M dwarfs and M giant stars (Luhman et al. 2003b). Figure 5 shows the Na I lines of M-type objects confirmed as members, superimposed on spectra of field dwarfs from Kirkpatrick et al. (1999), and of young M dwarfs from Luhman et al. (2003b) of the same spectral type. All these spectra were smoothed to the same resolution of 16 Å, and normalized in the range 8000–8400 Å. Both criteria used simultaneously offer a good membership indication. Additionally, the Av values obtained in this sample are in good agreement with the characteristic values measured in both subassociations by Briceño et al. (2007b, 345–360) for low-mass stars. Summarizing, M-type objects were classified as members if they showed Hα emission, Na I absorption clearly weaker than in field M dwarfs, and A_V consistent with the known values for each subassociation. The confirmed new members (three in OB1a and 19 in OB1b) are shown in Table 4. In the OB1a candidate sample we identified one late-type (M6) object from the field, and in OB1b we classified seven objects as field stars, four with late spectral types (M3, M5, M6, and M7) and three reddened early-type stars.

Taking our entire spectroscopic sample of 30 objects, we find that eight were classified as field stars (one out of four in OB1a and seven out of 26 in OB1b). Applying the exact test for the success rate in a binomial experiment (*R*-Statistical Software, Ihaka & Gentleman 1996), we find that the proportion of objects classified correctly as members is 0.73, with a

95% confidence interval of 0.54–0.87. Therefore, the selection technique described here correctly identifies 73.3% of objects.

5.2. Substellar Status

According to the models of Baraffe et al. (1998), objects with masses at the substellar limit (0.072 $M_{\odot}$) and ages between 7.9 Myr and 3.2 Myr (that correspond to the mean ages of OB1a and OB1b computed by Briceño et al. 2005 based on PMS low-mass stellar populations), have effective temperatures of 2936 K and 2993 K, respectively. Therefore, adopting the temperature to spectral-type relationship from Luhman et al. (2003b) the substellar limit at these ages corresponds to a spectral type between M6 (2990 K) and M6.5 (2935 K). Following this criterion, we consider as BDs those members with spectral types later than M6. In the Hectospec field located in the OB1a subassociation we confirmed one VLMS with spectral type M4.5, one VLMS at the substellar limit with spectral type M6, and one BD with a spectral type M7. In the Ori OB1b subassociation we identified 14 VLMSs, out of which seven have M6 spectral types, and five BDs (two with spectral types M6.5, two M7, and one M7.5).

6. T TAURI SIGNATURES ACROSS THE SUBSTELLAR LIMIT

The paradigm for low-mass star formation draws a picture in which a central low-mass star (T Tauri star) accretes mass from a circumstellar gas and dust disk, via magnetospheric accretion. Meanwhile the inner regions of the circumstellar disk are disrupted by the stellar magnetosphere, which then channels viscously accreting material out of the disk plane and toward the star along magnetic field lines (Königl. 1991; Shu et al. 1994). Signposts of this process, which have been directly observed in CTTSs, include: (a) IR emission from dust at a range of temperatures in the disk heated by stellar irradiation and viscous dissipation (from ∼1500 K at a few stellar radii, down to $\lesssim$50 K at ∼100 AU, e.g. Meyer et al. 1997; Hartmann 1998; Muzerolle et al. 2003); (b) blue/UV continuum excess emission from the accretion shock formed as accreting material falls onto the stellar surface (Valenti et al. 1993; Hartigan et al. 1995; Calvet & Gullbring 1998); (c) broad permitted emission lines produced in the ballistic magnetospheric gas flows (Muzerolle et al. 2001); and (d) forbidden emission lines produced in accretion-powered winds and jets (Hartigan et al. 1995).

Recent studies have searched for similar characteristics in the lowest-mass CTTSs and young BDs, as one way to ascertain whether similar formation mechanisms apply between both types of objects. There is indeed considerable evidence for magnetically-mediated disk accretion, including broad permitted emission-line profiles (especially Hα) and optical continuum veiling in BDs (e.g., White & Basri 2003; Muzerolle et al. 2005; Jayawardhana et al. 2003). Furthermore, the IR excess emission detected in many objects confirms the presence of irradiated circumstellar disks (Muench et al. 2001; Liu et al. 2003; Jayawardhana et al. 2003; Mohanty et al. 2004) and high-resolution observations of Hα emission allowed the measurements of the mass accretion rates in BDs (Muzerolle et al. 2000) resulting in a much lower value than stellar-mass CTTSs with similar ages (e.g., Muzerolle et al. 2005; Luhman et al. 2007, 443–457). It now seems well established that there is a continuum of CTTS-like properties across the substellar limit, shared by both the lowest-mass CTTSs and at least the higher-mass young BDs.

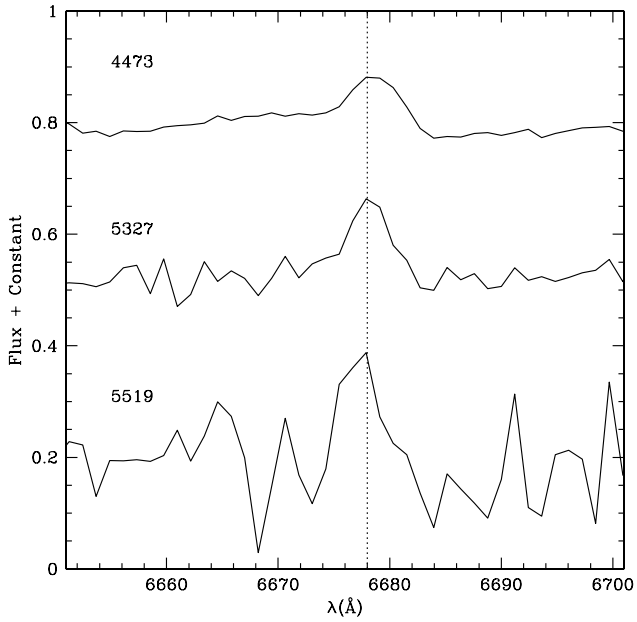

Figure 6. He I emission lines observed in 05345443-0144473, 05390532-0135327, and 05374145-0155519 supporting their classification as CTTSs.

Low-resolution spectra provide an appropriate means to look for Hα emission in CTTS. The dividing line between accreting (CTTSs) and non-accreting (WTTSs) was first set in terms of Hα emission at W(Hα) = −10 Å by Herbig & Bell (1988). More recently, White & Basri (2003) have revised this classification. In their new scheme, a star is considered to be a CTTS if W(Hα) $\leqslant$ −3 Å in the range K0–K5, W(Hα) $\leqslant$ −10 Å for K7–M2.5, W(Hα) $\leqslant$ −20 Å for M3–M5.5, and W(Hα) $\leqslant$ −40 Å for M6–M7.5. Here we followed their criteria to classify an object as a CTTS or a WTTS. Additionally Figure 6 shows the He I emission for the spectra in which this line was detected. Figure 7 shows the classification, with W(Hα) plotted as a function of the spectral type, with the CTTS/WTTS divide from White & Basri (2003) indicated by the dotted line. The results are summarized in Table 4.

7. DISKS AMONG THE WIDELY SPREAD PMS POPULATION OF ORION OB1

7.1. Trends in Accretion-Related Indicators

The fraction of objects exhibiting CTTS-like properties can be used as an indicator of the population of disk-bearing objects which are still accreting from circum(sub)stellar disks. How these numbers compare among samples with differing ages, but presumably sharing a common origin, can provide insight into the timescale for the shutting off of accretion near and below the substellar boundary.

Using the same disk indicators we consider here, the first determination of the CTTS and WTTS fractions for the low-mass, widespread stellar population in Orion by Briceño et al. (2005), over an area of ∼68 deg^2 showed that 11% of the members in OB1a and 23% of the members on OB1b are CTTS. More recently Briceño et al. (2007b, 345–360) found a lower-CTTS fraction of 6% in Ori OB1a and 13% in Ori OB1b. However, this study was restricted to a much smaller area (totaling ∼ 1.6 deg^2). It is worth noting that because there are regions with higher concentrations of CTTS, like the very young clusters

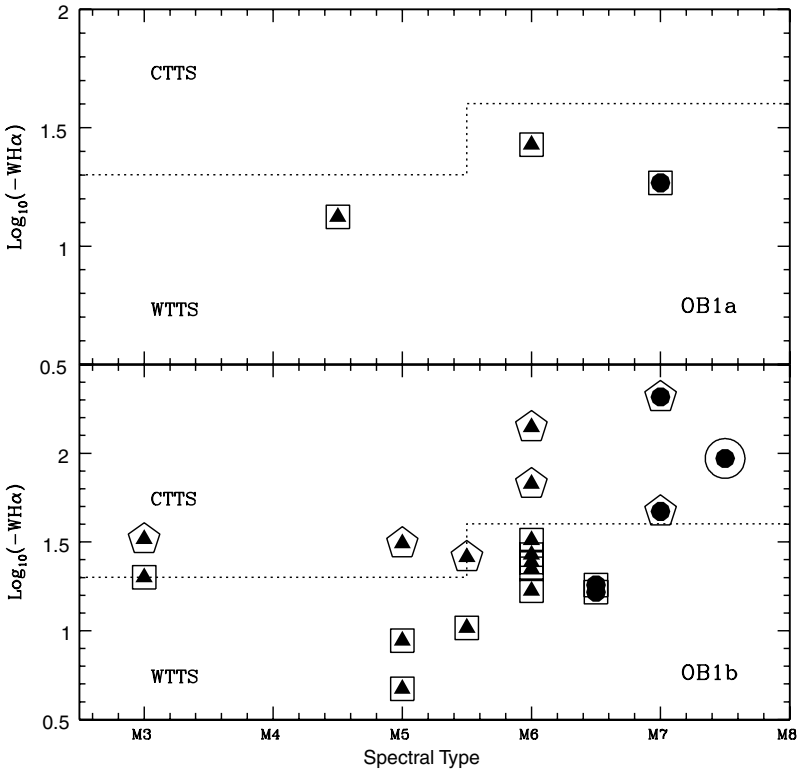

Figure 7. W(Hα) versus spectral type for the new members. The solid circles and triangles indicate BDs and VLMSs respectively, confirmed as new members. The squares represent members classified as WTTSs and pentagons indicate members classified as CTTSs. The dotted line indicates the separation between CTTSs and WTTSs from White & Basri (2003). The circled dot indicates member 05390910-0200267 that could not be classified as either a WTTS or CTTS as explained in Section 7.1.

NGC 2024/2068 located on the Orion molecular clouds (e.g., see Figures 5 and 6 of Briceño et al. 2005), the CTTS fraction on small spatial scales is strongly dependent on the location of the region being considered.

The very small size of our sample in OB1a (only three members) does not allow us to derive any meaningful estimate, other than saying that it is completely dominated by WTTSs. In OB1b, we find that seven of the 18 members that could be assigned a TTS type are CTTSs (because of suspected contamination from nebular emission, 05390910-0200267 could not be classified as either a WTTS or CTTS). If we again apply the exact test for the success rate in a binomial experiment (*R*-Statistical Software, Ihaka & Gentleman 1996), we find that the proportion of CTTSs in OB1b is 0.39, with a 95% confidence interval of 0.17–0.64; the large size of the confidence interval being due to the relatively small sample size. These results are largely consistent with previous findings, in the sense that the OB1a population is dominated by non-accreting PMS stars, whereas the accretor fraction in the younger OB1b region can be estimated in the range ∼13–40% depending on the region being considered and the sample size.

Our findings suggest that the overall number of accretors among VLMSs and BDs in OB1b is similar to that determined for low-mass ($M \gtrsim 0.3\,M_{\odot}$) stars by Briceño et al. (2005). Also, it seems that, as it happens in the low-mass PMS members, the VLMS/BD accretor fraction falls off by a significant amount once the population reaches ages ∼8–10 Myr. Determining the detailed evolution of the accretion fractions is similar between low-mass stars and VLMSs/BDs will require larger samples.

7.2. Near IR Disk Indicators

We analyzed the J-, H-, and K-band emission of all the new members confirmed in this work. Figure 8 shows the observational $J-H$ versus $H-K$ diagrams with the members classified as WTTSs and CTTSs. The members confirmed in OB1a (age ∼ 8 Myr) do not show excess emission in either color. In the ∼4 Myr old OB1b, where a fraction of the low-mass PMS stars ($M > 0.3\,M_{\odot}$) identified by Briceño et al. (2005) show IR excesses, 7/19 members confirmed in this work (one BD WTTS, four VLMS WTTSs, and two VLMS CTTSs) have $H-K > 0.45$ and lie on the right of the reddening line for an M6 star in Figure 8, the region expected for objects with excess emission produced by hot dust in the innermost part of the disk (∼0.1 AU; Meyer et al. 1997; Muzerolle et al. 2003). The resulting inner-disk fraction for the entire sample (VLMSs AND BDs) is 0.38, and using the exact test for the success rate in binomial experiments (*R*-Statistical Software, Ihaka & Gentleman 1996) we find a 95% confidence level interval 0.17–0.64. These numbers are very similar to what we found from disk accretion indicators (7.1), and consistent with the findings reported by Briceño et al. (2005).

Five of the new members confirmed in this work classified as WTTS VLMSs with masses ($0.08 < M/M_{\odot} < 0.4$) are located in the ∼1 deg^2 OB1b field studied with the *Spitzer Space Telescope* by Hernández et al. (2007b). Unfortunately, there are no similar observations for the objects we identified here in OB1a. For the five OB1b objects we have photometry in the four IRAC bands with the exception of 05312373-0150245, not detected in the [8.0] μm band. These five members have

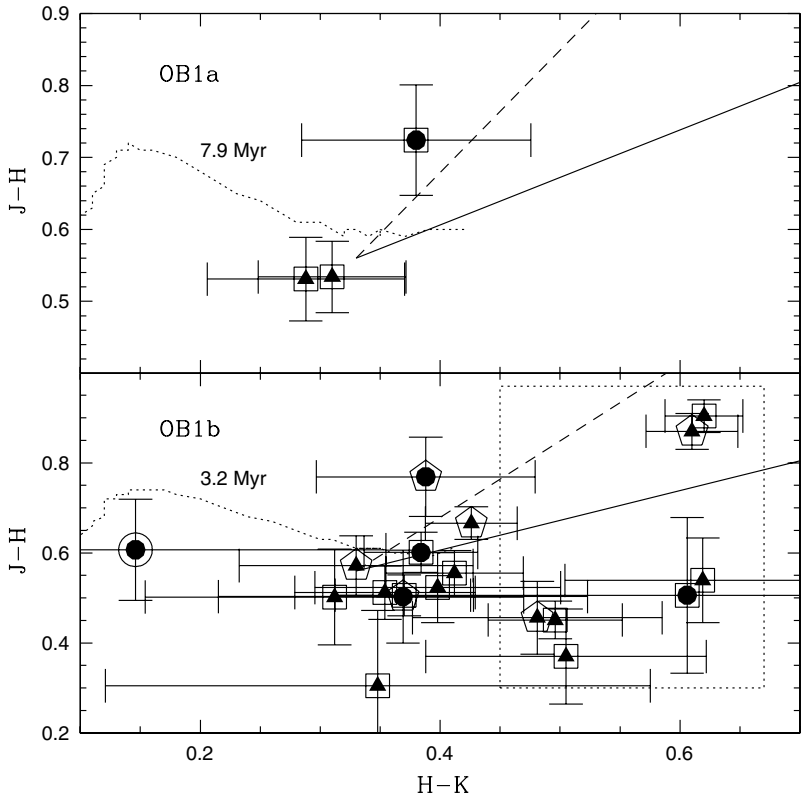

Figure 8. Observational $J - H$ versus $H - K$ diagram of the OB1a and OB1b members confirmed at this work. Symbols are as in Figure 7. The dotted lines represent the 7.9 Myr and 3.2 Myr isochrones from Baraffe et al. (1998) that correspond to the ages found by Briceño et al. (2005) on the basis of low-mass stars in each sub-association. The dashed line represents the reddening line for an M6 spectral type, and the dotted box encloses objects showing $H - K$ excess. The solid line is an extrapolation of the CTTS locus from Meyer et al. (1997) for early M stars to an M6 spectral type.

Table 5
IRAC Photometry of the New VLM Members of OB1b

ID-2MASS	STad	WHa	WTTS/CTTS	[3.6]	σ[3.6]	[4.5]	[σ4.5]	[5.8]	[σ5.8]	[8.0]	[σ8.0]
05300324-0138428	M3	−20.0	W	11.180	0.003	10.922	0.003	10.785	0.008	10.273	0.008
05311727-0136587	M6	−16.8	W	13.708	0.009	13.635	0.012	13.684	0.054	14.297	0.239
05312373-0150245	M6	−24.4	W	14.464	0.012	14.223	0.017	13.995	0.059	...	...
05322069-0125511	M5	−8.8	W	13.528	0.008	13.458	0.011	13.501	0.048	13.523	0.090
05323839-0127204	M5.5	−26.0	W	14.611	0.014	14.570	0.022	14.533	0.100	15.197	0.420

Note. Photometry is from Hernández et al. (2007b). Spectral types, W(Hα) and WTTS/CTTS classification are from our Table 4.

all been classified as WTTS and Table 5 provides the IRAC photometry. Figure 9 shows the [3.6]−[4.5] versus [4.5]−[5.8] and [3.6]−[4.5] versus [5.8]−[8.0] color–color diagrams with the excess region defined by Luhman et al. (2005) (left panel) and the photospheric and CTTS locus defined by Hartmann et al. (2005) (right panel). All the objects exhibit photospheric colors in both diagrams, consistent with their optical classification as non-accreting objects; the exception is 05300324-0138428, classified as a WTTS but whose [3.6]−[4.5] versus [5.8]−[8.0] colors fall within the CTTS locus defined by Hartmann et al. (2005), albeit offset toward smaller excess values.

Having only four objects in OB1b (all WTTSs) with full IRAC photometry prevents us from deriving a meaningful disk fraction; however, it is worth mentioning that for this same dataset Hernández et al. (2007b) derived a disk frequency of 13%, using ∼100 low-mass (∼0.3 $M_{\odot}$) PMS stars. Their determination agrees well with the CTTS fraction derived by Briceño et al. (2007b, 345–360) in the same area. Our inner-disk fraction of 38^{+26}_{-21}% (see above), obtained in an area approximately three times larger than that of Hernández et al. (2007b), is higher than their estimate, but consistent with the results from Briceño et al. (2005). As we have discussed in Section 7.1, the discrepancy could well be due, at least in part, to the largely non-uniform spatial distribution of disk-bearing CTTSs in OB1.

In the young σ Orionis cluster (age ∼ 3 Myr), Caballero et al. (2007) combined optical, near-IR, and *Spitzer* IRAC/MIPS measurements to derive a disk fraction of ∼50% in a sample of 30 BDs down to $M \sim 0.015\ M_{\odot}$. However, this sample is a mixture of spectroscopically confirmed members and candidates selected on the basis of photometry only. If we restrict the analysis to the 13 objects in their Table B.1 which have spectral types, in the range M6–M7.5 (a spectral-type range that overlaps the sample in this work), we find that only five objects exhibit

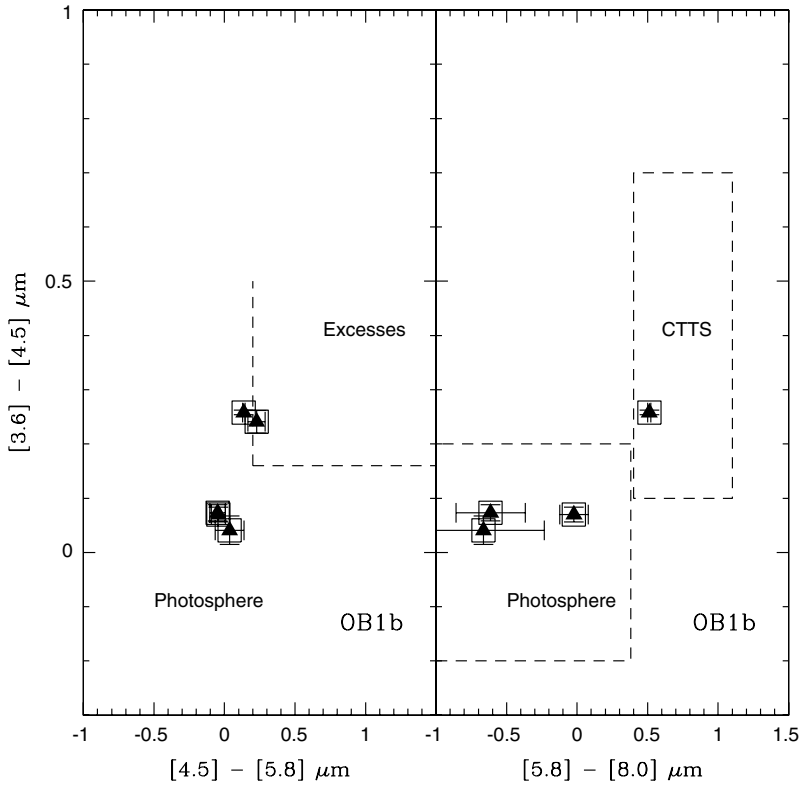

Figure 9. Color–color diagrams of the five OB1b members with available IRAC photometry. The dashed lines in the left panel indicate the region of excess IR emission defined by Luhman et al. (2005). The dashed boxes in the right panel indicate the position of the photospheric locus and the Class II source locus from Hartmann et al. (2005). Symbols are as in Figure 8.

excess IR emission that can be attributed to circum(sub)stellar disks. This produces a somewhat lower disk fraction of 38%, which agrees very well with the value we found above, from the near-IR disk indicators.

As in the case of the accretion-related indicators, our results from the *JHK* 2MASS photometry suggest that (1) disk fractions are similar in VLMS/BD and the lower-mass PMS stars ($M \gtrsim 0.3 M_{\odot}$) at a given age; (2) the disk fraction near the substellar boundary falls off significantly, as occurs for the lower-mass stars ($0.8 \lesssim M/M_{\odot} \lesssim 0.3$), during the period ∼4–8 Myr. However, the present small size of the available samples precludes any detailed analysis on how these fractions may evolve on both sides of the substellar limit.

We want to remark that strictly following the classification scheme by White & Basri (2003), of the seven objects which show IR excesses, namely 05300324-0138428, 05312373-0150245, 05350579-0121443, 05322069-0125511, 05340726-0149380, 05345443-0144473, and 05390054-0150469, only the last two have been classified as CTTSs. Object 05300324-0138428 shows an Hα-emission equivalent width at the WTTS/CTTS limit in Figure 7, and its IRAC colors place it at the borderline between photospheric colors and IR excesses on both color–color diagrams of Figure 9. A similar situation is that of 05312373-0150245, which is located near the WTTS/CTTS boundary in Figure 7, given our 0.5 subclass uncertainty in the spectral-type classification, and its IRAC colors suggest it may have a small IR excess. Objects 05322069-0125511 and 05340726-0149380 have Hα-emission equivalent widths well below the WTTS/CTTS boundary. We have IRAC photometry only for 05322069-0125511, and its colors are clearly photospheric. In the near-IR *JHK* diagram (Figure 8) both objects have the smallest $H - K$ values among the "excess emission" objects, lying closest to the $H - K = 0.45$ limit of our *JHK* excess box. BD 05350579-0121443 whose J, H, and K magnitudes are among the faintest of the sample, has an "ABB" 2MASS photometric flag which indicates a lower S/N in the H- and K-bands, and hence a larger uncertainty in the $H - K$ color. We conclude that, of the five objects classified as WTTS but showing IR excess, four have Hα equivalent widths, from our low-resolution spectra, that place them on or close to the border between WTTS and CTTS types. High-resolution spectroscopy will be needed to analyze the Hα line profile and determine the presence of line wings extending to large velocities, characteristic of accreting stars (e.g., Muzerolle et al. 2005).

Of the seven objects classified as CTTS only two fall within the IR excess box in Figure 8. However, three out of the five CTTS outside the box have large enough 1σ error bars that would bring them into the excess emission region. Therefore, within errors, only two CTTSs really seem to lack IR excess emission at *JHK*. This is consistent with findings for VLMSs in other star-forming regions such as Taurus (Luhman et al. 2003a). Observations at longer wavelengths should allow us to detect excess IR emission in these two objects.

8. REDDENING AND H-R DIAGRAMS

The extinction toward each object was estimated from the $I - J$ color, for which possible contributions from excess emission at short and long wavelengths are minimized (Luhman et al. 2003b). In order to compute the intrinsic colors as a

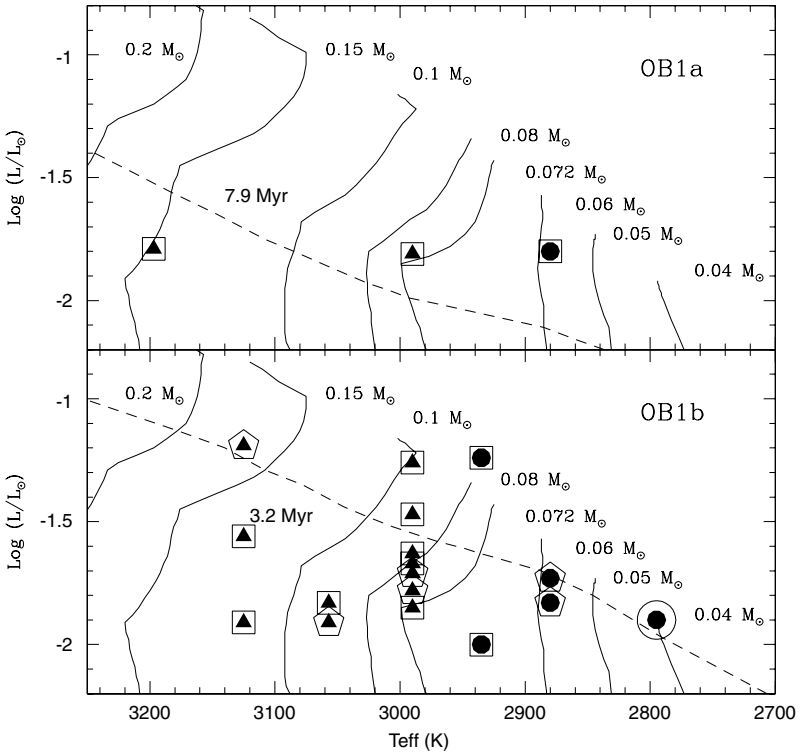

Figure 10. $H - R$ diagrams of confirmed members located in Hectospec OB1a and OB1b fields. Symbols are as in Figure 7. Evolutionary tracks and isochrones are from Baraffe et al. (1998) where the 3.2 Myr and 7.9 Myr isochrones correspond to the ages of OB1a and of OB1b respectively, computed from the low-mass members ($M > 0.3 M_{\odot}$) in color–magnitude diagrams by Briceño et al. (2005).

function of spectral type, we interpolated the corresponding temperature from the spectral-type–temperature relationship of Luhman et al. (2003b), into the Baraffe et al. (1998) models corresponding to ages of 7.9 Myr for OB1a, and 3.2 Myr for OB1b.

The resulting intrinsic colors and computed extinctions are listed in Table 4. Extinctions are in the range $0.6 < A_V < 0.9$ for OB1a and $0.1 < A_V < 3.9$ for OB1b consistent with previously reported values in both regions by Briceño et al. (2005). Bolometric magnitudes were calculated using absolute I-band magnitudes M_I and the bolometric correction $\mathrm{BC}_I = 0.02 + 0.575(V - I) - 0.155(V - I)^2$ from Legget et al. (1996) where $V - I$ is the intrinsic color from Kenyon & Hartmann (1995). Figure 10 shows the resulting H-R diagrams and Table 4 the mass estimates that result from the interpolation of luminosities and temperatures within the Baraffe et al. (1998) models. The mean ages derived are $\sim 4 \pm 2$ Myr and $\sim 8 \pm 2$ Myr for OB1a and OB1b respectively, in good agreement with ages derived based on low-mass stars (Briceño et al. 2005).

9. SUMMARY AND CONCLUSIONS

We have presented initial results of our search for substellar objects and VLMSs in the widely dispersed populations of the Orion OB1a and OB1b subassociations. Our results can be summarized as follows.

1. Using deep optical I-band photometry and data from the 2MASS survey, we constructed optical-IR color–color and color–magnitude diagrams, in which we selected candidates across ~ 14.8 deg^2 in Ori OB1 and over ~ 6.7 deg^2 in Ori OB1b with completeness down to $0.05\,M_{\odot}$ with $A_V \leqslant 0.6$ for OB1a, and $0.072\,M_{\odot}$ with $A_V \leqslant 2$ for OB1b. We obtained low-resolution optical spectra for a subsample of four candidates over ~ 0.8 deg^2 of OB1a, and 26 candidates within ~ 2.5 deg^2 of OB1b.
2. Through spectral signatures we confirmed three new members in OB1a, one of which is clearly substellar (spectral type M7, with an inferred mass $\sim 0.06\,M_{\odot}$) and two are VLMSs, one of which is at the substellar limit (spectral type M6, with mass $M \sim 0.072\,M_{\odot}$). In OB1b we found 19 new members: 14 are VLMSs, of which seven are at the substellar limit, and five are substellar members with spectral types between M6.5 and M7.5. From the spectroscopy we find that our photometric candidate selection technique is highly efficient (73%) in picking out young, very low mass and substellar members of the Orion OB1 association. Masses were estimated according to the Baraffe et al. (1998) models, and the less-massive member (M7.5 spectral type) has an estimated mass $M \sim 0.04\,M_{\odot}$.
3. The new members have been classified as CTTSs or WTTSs following the scheme of White & Basri (2003). We found that all three members confirmed in OB1a are WTTSs, while 39^{+25}_{-22}% of the members in OB1b are CTTSs. These results are largely consistent with recent findings, in the sense that the OB1a population is dominated by non-accreting PMS stars, whereas the accretor fraction in the younger OB1b region can be estimated in the range $\sim$13–40% depending on the exact location and area being considered, and the sample size. Our findings indicate that in OB1b, the number of accretors in VLMSs/BDs is similar to that derived for low-mass PMS stars (Briceño et al. 2005); also, that the overall number of accretors, both in low-mass stars and among VLMSs/BDs falls off by a significant amount by ages $\sim 8 - 10$ Myr.

4. Of the 19 newly confirmed members of Ori OB1b, seven (one BD WTTS, four VLMS WTTSs, and two VLMS CTTSs) exhibit excess emission in the 2MASS $H-K$ color as would be expected of thermal emission from hot dust in the innermost part of a circumstellar disk. None of the three Ori OB1a members shows near-IR excesses. We derive an inner-disk fraction of 38^{+26}_{-21}%, which is in excellent agreement with our result for the accretor fraction. Our inner-disk estimate for VLMSs and BDs is also consistent with the results from Briceño et al. (2005) for higher-mass stellar objects ($M \gtrsim 0.3\,M_{\odot}$), and with findings for BDs spectroscopically confirmed in σ Ori by Caballero et al. (2007). The few Ori OB1b members with *Spitzer* data are all WTTSs, by optical indicators; the IRAC photometry is largely consistent with this classification. Only one object shows marginal indication of excess emission at 8 μm.
   As in the case of the accretion-related indicators, the near-IR indicators suggest that (1) at a given age, the inner-disk fraction of objects at/near the substellar boundary is similar to that determined in the lower-mass ($M \gtrsim 0.3\,M_{\odot}$) PMS stars; (2) the inner-disk fraction seems to fall off significantly, both in VLMSs/BDs and low-mass stars, once the population has aged to $\sim$8 Myr, as in Ori OB1a. However, the present small size of the available samples precludes any detailed analysis on how these fractions may evolve on both sides of the substellar limit.
5. Finally we comment on the discovery of two new members 05335219-0156398 (M7) and 05390532-0135327 (M6) classified as CTTSs, without contamination by emission lines from the cloud, both exhibiting strong Hα emission, with W(Hα) $\lesssim -140$ Å, suggesting significant ongoing accretion.

This work has been supported in part by grant S1-200101144 of FONACIT, Venezuela. J.J.D., acknowledges support from grant 200400829 from FONACIT, Venezuela. We thank Kevin Luhman for useful comments during the spectral classification, Nelson Caldwell for supplying us with the response curve of Hectospec, and Susan Tokarz, who is in charge of the reduction and processing of Hectospec spectra. This publication makes use of data products from the 2MASS, which is a joint project of the University of Massachusetts and the Infrared Processing and Analysis Center/California Institute of Technology, funded by the National Aeronautics and Space Administration and the NSF. This research has also been benefitted from the M, L, and T dwarf compendium housed at DwarfArchives.org and maintained by Chris Gelino, Davy Kirkpatrick, and Adam Burgasser, from the ADS article retrieving service, and the Sistema de Colección de Datos Observacionales SCDOBS (Ponsot et al. 2007). We thank the assistance of the personnel, observers, telescope operators, and technical staff at CIDA and FWLO, who made possible the observations at the Jürgen Stock Schmidt-type telescope of the Venezuela National Astronomical Observatory (OAN) and at the MMT telescope at Fred Lawrence Whipple Observatory (FLWO) of the Smithsonian Institution. Finally, we acknowledge the comments from an anonymous referee, which helped improve this article.

REFERENCES

Bally, J., Stark, A. A., Wilson, R. W., & Langer, W. D. 1987, ApJ, 312, L45
Baltay, et al. 2002, PASP, 114, 780
Barrado y Navascués, D., Béjar, V. J. S., Mundt, R., Martín, E. L., & Rebolo, R. 2003, A&A, 404, 171
Barrado y Navascués, D., & Martin, E. 2003, AJ, 126, 2997–3006
Baraffe, I., Chabrier, G., Allard, F., & Hausschildt, P. H. 1998, A&A, 337, 403
Béjar, V. J. S., Zapatero-Osorio, M. R., & Rebolo, R. 1999, ApJ, 521, 671
Béjar, V. J. S., et al. 2001, ApJ, 556, 830
Briceño, C., Calvet, N., Hernández, J., Vivas, A. K., Hartmann, L., Downes, J. J., & Berlind, P. 2005, AJ, 129, 907
Briceño, C., Hartmann, L., Hernández, J., Calvet, N., Vivas, A. K., Furesz, G., & Szentgyorgyi, A. 2007a, ApJ, 661, 1119
Briceño, C., Hartmann, L. W., Stauffer, J., Gagné, M., Stern, R., & Caillault, J. 1997, AJ, 113, 740
Briceño, C., Luhman, K. L., Hartmann, L., Stauffer, J. R., & Kirkpatrick, D. 2002, ApJ, 580, 317
Briceño, C., Preibisch, T., Sherry, W. H., Mamajek, E. A., Mathieu, R. D., Walter, F. M., & Zinnecker, H. 2007b, in Protostars & Planets V., ed. B. Reipurth, D. Jewitt, & K. Keil (Tucson, AZ: Univ. Arizona Press)
Briceño, C., et al. 2001, Science, 291, 93
Caballero, J. A., Béjar, V. J. S., Rebolo, R., & Zapatero-Osorio, M. R. 2004, A&A, 424, 857
Caballero, J. A., et al. 2007, arXiv:0705.0922
Calvet, N., & Gullbring, E. 1998, ApJ, 509, 802
Calvet, N., Briceno, C., Hernandez, J., Hoyer, S., Hartmann, L., Sicilia-Aguilar, A., Megeath, T., & D'Alessio, P. 2005, AJ, 129, 935
Cardelli, J. A., Clayton, G. C., & Matis, J. S. 1989, ApJ, 345, 245
Fabricant, D. G., Hertz, E. N., Szentgyorgyi, A. H., Fata, R. G., Roll, J. B., & Zajac, J. M. 1998, Proc. SPIE, 3355, 285
Fan, X., et al. 2000, AJ, 119, 928
Gelino, C. R., Kirkpatrick, J. D., & Burgasser, A. J. 2004, Bull. AAS, 36, 1354 (http://DwarfArchives.org)
Genzel, R., & Stutzki, J. 1989, ARA&A, 27, 41
González-García, B. M., Zapatero Osorio, M. R., Béjar, V. J. S., Bihain, G., Barrado, Y., Navascués, D., Caballero, J. A., & Morales-Calderón, M. 2006, A&A, 460, 799
Hartmann, L. 1998, Accretion Processes in Star Formation (Cambridge: Cambridge Univ. Press)
Hartmann, L., Megeath, S. T., Allen, L., Luhman, K., Calvet, N., D'Alessio, P., Franco-Hernandez, R., & Fazio, G. 2005, ApJ, 629, 881–896
Hartigan, P., Edwards, S., & Ghandour, L. 1995, ApJ, 452, 736
Herbig, G. H., & Bell, K. R. 1988, Lick Observatory Bulletin (Santa Cruz, CA: Lick Observ.)
Hernández, J., Calvet, N., Briceño, C., Hartmann, L., & Berlind, P. 2004, AJ, 127, 1682
Hernández, J., et al. 2007a, ApJ, 662, 1067
Hernández, J., et al. 2007b, ApJ, 671, 1784
Hillenbrand, L. A., & Carpenter, J. M. 2000, ApJ, 540, 236
Ihaka, R., & Gentleman, R. 1996, J. Comput. Graphic. Stat., 5, 299–314
Jayawardhana, R., Ardila, D. R., Stelzer, B., & Haisch, K. E. 2003, AJ, 126, 1515
Jayawardhana, R., Mohanty, S., & Basri, G. 2002, ApJ, 578, 141
Kenyon, S., & Hartmann, L. ApJS, 101, 117
Kenyon, M. J., Jeffries, R. D., Naylor, T., Oliveira, J. M., & Maxted, P. F. L. 2005, MNRAS, 356, 89
Kirkpatrick, J. D., et al. 1999, ApJ, 519, 802
Königl, A. 1991, ApJ, 370, L39
Landolt, A. U. 1992, AJ, 104, 340
Legget, S. K., Allard, F., Berriman, G., Dahn, C. C., & Hauschildt, P. 1996, ApJS, 104, 117
Liu, M. C., Najita, J., & Tokunaga, A. T. 2003, ApJ, 585, 372
Luhman, K., et al. 2005, ApJ, 631, L69
Luhman, K. L. 2004, ApJ, 602, 816
Luhman, K. L., Briceño, C., Stauffer, J. R., Hartmann, L., Barrado y Navascués, D., & Nelson, C. 2003a, ApJ, 590, 348
Luhman, K. L., Joergens, V., Lada, C., Muzerolle, J., Pascucci, I., & White, R. 2007, in Protostars & Planets V., ed. B. Reipurth, D. Jewitt, & K. Keil (Tucson, AZ: Univ. Arizona Press), 443–457
Luhman, K. L., Stauffer, J. R., Muench, A. A., Rieke, G. H., Lada, E. A., Bouvier, J., & Lada, C. J. 2003b, ApJ, 593, 1093
Maddalena, R. J., Morris, M., Moscowitz, J., & Thaddeus, P. 1986, ApJ, 303, 375
Meyer, M. R., Calvet, N., & Hillenbrand, L. A. 1997, AJ, 114, 288
Mink, D. J. 1999, ASP Conf. Ser., 172, 498–501
Mohanty, S., & Jayawardhana, Basri, G. 2005, ApJ, 498, 522
Mohanty, S., Jayawardhana, R., Natta, A., Fujiyoshi, T., Tamura, M., & Barrado y Navascués, D. 2004, ApJ, 609, L33
Monet, D., et al. 1998, PMM USNO-A2.0 Catalog (Washington, DC: USNO)
Muench, A. A., Alves, J., Lada, C. J., & Lada, E. A. 2001, ApJ, 558, L51
Muzerolle, J., Briceno, C., Calvet, N., Hartmann, L., Hillenbrand, L., & Gullbring, E. 2000, ApJ, 141, 144

Muzerolle, J., Calvet, N., & Hartmann, L. 2001, ApJ, 550, 944
Muzerolle, J., Calvet, N., Hartmann, L., & D'Alessio, P. 2003, ApJ, 597, L149
Muzerolle, J., Luhman, K., Briceño, C., Hartmann, L., & Calvet, N. 2005, ApJ, 625, 906
Oppenheimer, B. R., Kulkarni, S. R., & Stauffer, J. R. 2000, in Protostars and Planets IV, ed. V. Mannings, A. P. Boss, & S. S. Russell (Tucson, AZ: Univ. Arizona Press), 1313
Ponsot, E. A., Briceño, C., & Vivas, A. K. 2007, Interciencia, 32, 76
Preibisch, T., et al. 2005, ApJS, 160, 582
Reipurth, B., & Clarke, C. 2001, AJ, 122, 432
Schlegel, D. J., Finkbeiner, D. P., & Davis, M. 1998, ApJ, 500, 525
Sherry, W. H., Walter, F. M., & Wolk, S. J. 2004, AJ, 128, 2316
Shu, F., Najita, J., Ostriker, E., Wilkin, F., Ruden, S., & Lizano, S. 1994, ApJ, 429, 781
Sicilia-Aguilar, A., Hartmann, L., Hernandez, J., Briceno, C., & Nuria, 2005, AJ, 188, 209
Slesnick, C. L., Hillenbrand, L. A., & Carpenter, J. M. 2005, ApJ, 625, 1063
Valenti, J. A., Basri, G., & Johns, C. M. 1993, AJ, 106, 2024
Warren, W. H., & Hesser, J. E. 1977, ApJS, 34, 115
White, R. J., & Basri, G. 2003, ApJ, 582, 1109